ChemComm

COMMUNICATION

View Article Online
View Journal | View Issue

Cite this: *Chem. Commun.*, 2014, **50**, 3838

Received 11th February 2014,
Accepted 22nd February 2014

DOI: 10.1039/c4cc01079e

www.rsc.org/chemcomm

Spin crossover intermediate plateau stabilization in a flexible 2-D Hofmann-type coordination polymer†

Y. Maximilian Klein,[ab] Natasha F. Sciortino,[a] Florence Ragon,[a] Catherine E. Housecroft,[b] Cameron J. Kepert[a] and Suzanne M. Neville*[a]

The abrupt and hysteretic two-step spin crossover in a new triazole-based 2-D Hofmann-type complex shows a record breaking 120 K intermediate plateau (IP) region stabilized by negative cooperative interactions.

Spin crossover (SCO) complexes are of current interest because of their potential use in advanced technologies, such as memory storage devices and molecular sensing.[1–5] Many of these applications require hysteretic and abrupt complete SCO transitions centred around or near room temperature.[1,3–5] To prepare materials with optimal properties and then transform them into functional and purposeful materials we must fully understand the link between structure and function.[6] This is why many SCO studies reported include detailed structural analysis coupled with magnetic studies with an eye towards fine tuning solid state structural features such as intra- and intermolecular interactions, which are of key consequence in attaining lattice cooperativity. Using such information, recent studies have taken steps towards the incorporation of SCO materials into useful devices through probing the effect of miniaturisation on long-range communication by preparing, for example, nanoparticles, nanocrystals and thin layers.[7–10]

There are varied SCO behaviour characters which are possible, such as complete, incomplete, abrupt, gradual one-step and multi-step transitions, and each are well documented in the literature.[2,11] Multi-step transitions, *i.e.* those that display three- or more regions of thermally stable, distinct magnetic states (*e.g.* HS–HS, HS–LS, LS–LS, HS = high spin, LS = low spin), are a recent feature in the literature owing to the enhanced possibilities these materials provide for additional information storage capacity (ref. 12–21 and references therein). The most simplistic structural feature that enables a multi-step transition is the presence of two- (or more) structurally and magnetically inequivalent SCO sites. Such structural deviations may be subtle, such as in the dinuclear material $[Fe_2^{II}(ddpp)_2(NCS)_4]\cdot 4CH_2Cl_2$ (ddpp = 2,5-di(2′,2″-dipyridylamino)pyridine), for which the coordinative linkage of SCO sites generates slight iron(II) site inequivalence,[22] or dramatic, such as in the hybrid material $[Fe^{II}(dpp)_2][Ni(mnt)_2]\cdot MeNO_2$ (dpp = 2,6-bis(pyrazol-1-yl)pyridine), which undergoes multiple spin-state conversions of both components.[13] An alternative, or additional path to multi-stability is through an accompanying symmetry-breaking event triggered by or coincident with SCO. There are several recent examples of this type, such as $[Fe^{III}(nsal_2trien)]SCN$ and $[Fe^{III}(L2)]ClO_4$, which show long-range order at the IP owing to a symmetry conversion.[18,23]

We are interested in designing a rational platform for routinely achieving multi-stability and then exploiting this to systematically tune and optimize multi-stable SCO properties. The multi-stable magnetic characters to optimize include: abrupt and hysteretic transitions; high transition temperatures; and large regions of thermal stability for each step.[3] Towards attaining abrupt and hysteretic transitions with high transition temperatures, we focus here on the Hofmann-type framework system, comprised of $[Fe^{II}M^{II}(CN)_4]$ 2-D grids (M^{II} = Pt, Pd, Ni) linked or separated by aromatic N-donor ligands.[16,19,24–32] These systems show high SCO cooperativity, facilitated by the bimetallic layered structure and furthermore, provide a flexible platform for fine-tuning inter- and intra-molecular interactions *via* synthetic manipulation of the interlayer spacing (host or guest related). Importantly, multi-step transitions are a conceptually proven target feature in Hofmann-type materials due to the distortable nature of the bimetallic layer largely driven by solid state interactions.[16,17,19,29,32,33] The generation of inequivalent SCO sites can be conceivably targeted in Hofmann-type materials through exploiting the connectivity in the interlayer spacing, *i.e.* the incorporation of ligands with unsymmetric binding mode and/or interaction sites. Whilst to date the majority of Hofmann-type materials have focused on pyridyl N-donor ligands[33] we utilize a 1,2,4-triazole group which through its monodentate binding mode provides a less symmetric ligand coordination environment. This binding furthermore generates multiple (unsymmetric) interaction site possibilities *via* the unbound atoms. Finally, in choosing this type of ligand

[a] *School of Chemistry, The University of Sydney, Sydney, NSW, 2006 Australia. E-mail: suzanne.neville@sydney.edu.au*

[b] *Department of Chemistry, University of Basel, Spitalstrasse 51, CH-4056, Switzerland*

† Electronic supplementary information (ESI) available: Experimental, single crystal and powder X-ray diffraction. CCDC 963504–963506. For ESI and crystallographic data in CIF or other electronic format see DOI: 10.1039/c4cc01079e

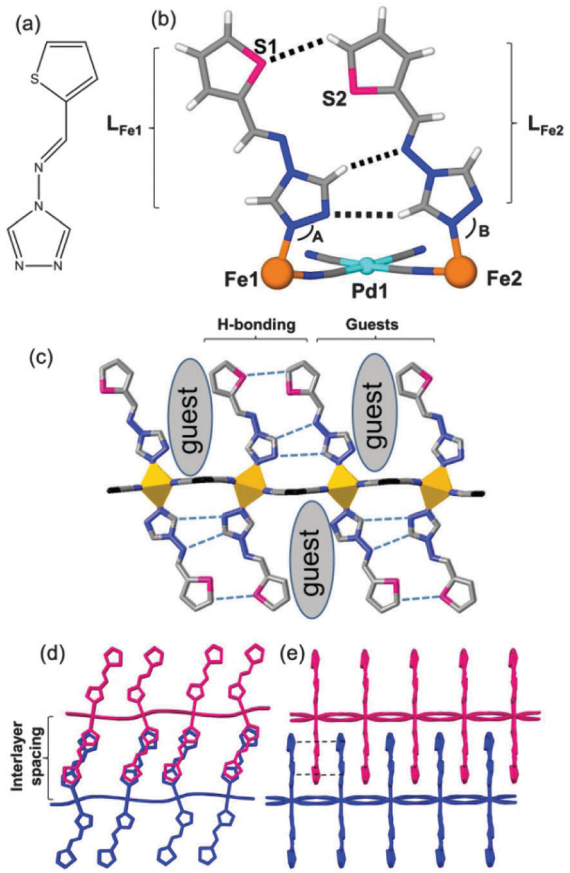

Fig. 1 (a) *N*-Thiophenylidene-4*H*-1,2,4-triazol-4-amine (thtrz), (b) the asymmetric unit of **1** (excluding solvent molecules), (c) a 2-D layer with ligand interactions and larger guest-filled spaces. (d and e) Adjacent layers inter-digitate with ligand π-stacking interactions (---).

platform we can tailor the interactions (host–host or host–guest) in the interlayer space with a specific interest towards stabilizing mixed HS–LS species to attain large thermally stable IP regions.

The material $[Fe(thtrz)_2Pd(CN)_4]\cdot(EtOH)(H_2O)$ (thtrz = *N*-thiophenylidene-4*H*-1,2,4-triazol-4-amine, Fig. 1(a)), **1**, is readily formed as single crystals or a pure bulk polycrystalline powder. Full single-crystal structural analysis at 260 K revealed $Fe^{II}N_6$ octahedral environments coordinated equatorially by N-donor $[Pd(CN)_4]^{2-}$ metallo-ligands and axially to terminal N1-donor thtrz ligands (Fig. 1(b)). The overall structure motif adopted, of a 2-D inter-digitated pillared-layered Hofmann-type topology, consists of undulating 2-D $[FePd(CN)_4]$ grids separated by thtrz ligands (Fig. 1(c)). The layers stack such that the thtrz ligands align in an eclipsed face-to-face fashion generating an array of π–π interactions and defining a pseudo 3-D character (Fig. 1(d and e)). The structurally distinct iron(II) sites (**Fe1** and **Fe2**) and associated ligands ($\mathbf{L_{Fe1}}$ and $\mathbf{L_{Fe2}}$, Fig. 1(b)) are generated by self-complementary hydrogen-bonding interactions between pairs of ligands which direct the ligand geometry by 'locking-in' the Fe–N–N(trz) angle (Fig. 1(b) **A** and **B**, Table 1). Notably, this results in vastly different angles of ligand approach into the interlayer spacing and generates alternating regions of ligand hydrogen-bonding and guest-filled 1-D pores (Fig. 1(c)). The guests are additionally involved in intermolecular interactions with the host framework (Fig. S5, ESI†).

Table 1 Selected single crystal structural parameters

Parameters (**Fe1**, **Fe2**)	100 K	180 K	260 K
Fe^{II} spin state	LS, LS	HS, LS	HS, HS
Σ^a (°)	9.2, 4.4	21.2, 1.2	11.3, 5.4
$\langle d_{Fe-N}\rangle^b$ (Å)	1.95, 1.94	2.15, 1.95	2.15, 2.16
Fe–N–N(trz)^c (°) (**A**, **B**)	125.1, 121.8	130.7, 122.2	131.3, 121.3
Fe–N(C)$_4$ tilt^d (°)	16.73, 9.31	22.09, 8.36	20.44, 9.65

^{a} Octahedral distortion parameter calculated by sum of $|90 - \theta|$ for the twelve *cis*-N–Fe–N angles in the octahedron.[5] ^{b} Average Fe–N distance. ^{c} Fe–N–N(trz) angle (**A** and **B**, as defined in Fig. 1(b)). ^{d} Equatorial out-of-plane octahedral tilt angle.

The single crystal structural data collected at 260 K reveal that both **Fe1** and **Fe2** are in the HS state ($d_{\langle Fe-N\rangle}$, Table 1) and that the coordination environment of **Fe1** is considerably more distorted than that of **Fe2**, which displays an almost perfect octahedron (octahedral distortion parameter, $\Sigma_{Fe\text{-}1}$: 14.4°, $\Sigma_{Fe\text{-}2}$: 3.2°, Table 1). This large distortive difference indicates that a multi-step (or half-step) transition is possible as with cooling the HS to LS transition will be considerably less favoured for **Fe2** than **Fe1**.[6] Further exemplifying the greater distortion to **Fe1** than **Fe2** is the more pronounced octahedral tilt out of the $[FePd(CN)_4]$ plane evident both visually (Fig. 1(c)) and quantitatively (Table 1). Subsequent magnetic susceptibility measurements indeed reveal a striking multi-stable character detailing an abrupt and hysteretic two-step SCO with a record-breaking IP region of 120 K (Fig. 2(a)).[14] Detailing the magnetic curve, the $\chi_M T$ values remain constant at *ca.* 3.4 $cm^3\ mol^{-1}\ K$ with cooling from room temperature, indicating that iron(II) exists in the HS state, until 230 K, where there is a rapid

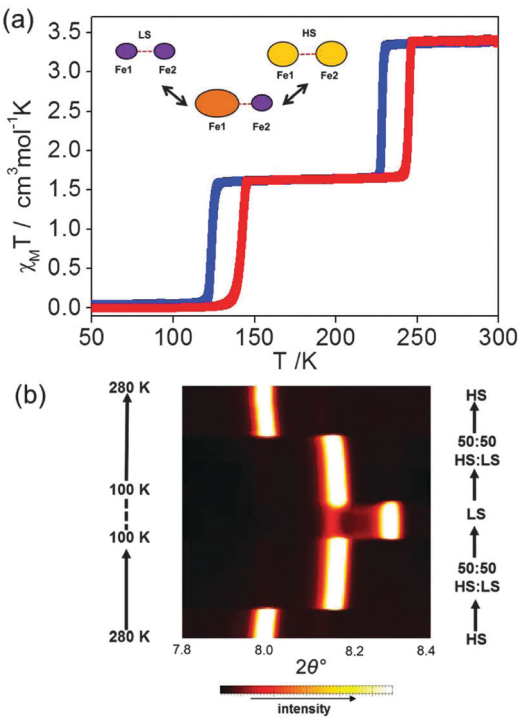

Fig. 2 (a) $\chi_M T$ *versus* temperature (1 K min^{-1}) for **1** (cooling (blue) and heating (red) curves). Inset: schematic of HS(yellow)–HS to HS–LS(purple) to LS–LS transition of **Fe1** and **Fe2** (interactions —). (b) Variable temperature synchrotron powder X-ray diffraction data single peak evolution over the range 7.8–8.4°.

drop in $\chi_M T$ to 1.6 cm^3 mol^{-1} K. This value remains constant until 130 K where there is a further rapid decrease in $\chi_M T$ to 0.05 cm^3 mol^{-1} K representing a complete spin state conversion of iron(II) sites to LS. The heating curve shows the same two-step SCO behaviour with hysteresis loops of 19 K ($T_{1/2}\downarrow$: 123 K $T_{1/2}\uparrow$: 142 K) and 16 K ($T_{1/2}\downarrow$: 228 K $T_{1/2}\uparrow$: 244 K). The IP corresponds to a 50 : 50 ratio of HS and LS iron(II) sites distributed in the crystalline lattice.

To gain an overall perspective of the structural changes accompanying the two-step switching in variable temperature synchrotron-based powder X-ray diffraction was used and most notably revealed a single-phase behaviour over the entire SCO temperature range (Fig. 2(b)). The powder diffraction data additionally revealed pronounced, abrupt shifts in Bragg reflections that mirror the magnetic data (Fig. S11, ESI†). Most importantly, parallel single crystal data collected at the IP (180 K) and LS state (100 K) confirm the iron(II) spin state progression (HS–HS to HS–LS to LS–LS, respectively, for **Fe1**–**Fe2**) and reveal definitively the underlying fundamental reason for the prolonged thermal existence of the IP region. Surprisingly, with cooling from 260 to 180 K, concomitant with the HS to LS transition at **Fe2**, the octahedral distortion of **Fe1** increases dramatically (11.3 → 21.2°, Fig. 2(a) inset). Additionally, the sequence of octahedral distortion of **Fe2** with heating from 100 to 180 K (4.4 → 1.2°) indicates that the LS to HS transition at **Fe1** stabilises the LS state at **Fe2**. In particular, with each respective HS ↔ LS transition at either **Fe1** or **Fe2**, as the Fe–N bond lengths and overall octahedral volume vary this causes a mechano-elastic stress resulting in stabilization through distortive forces and thus significantly enhancing the temperature stability range of the IP region. We attribute these findings to a negative cooperative impact imparted by the hydrogen-bonding network interconnecting the ligands associated with **Fe1** and **Fe2** which inhibits the entire lattice converting from HS to LS in one-step. Negative cooperativity has been noted previously, for example in dinuclear materials in which the lower temperature HS to LS transition is completely inhibited, resulting in a half one-step SCO.[34,35]

In summary, we have shown that the combination of 2-D Hofmann-type materials and aromatic ligands with inherent binding asymmetry can promote the formation of structurally and magnetically distinct SCO sites towards predictably attaining multi-step SCO behaviours. Furthermore, we highlight that interconnecting spin switching sites can facilitate negative cooperativity and stabilize IP regions, where here a remarkable 120 K IP has been achieved by this method. We are currently looking into the host–guest properties within these flexible 2-D porous materials which promise adaptable and versatile structure-function response.

This work was supported by a Fellowships and Discovery Project funding from the Australian Research Council. Use of the Advanced Photon Source was supported by the U.S. Department of Energy, Office of Science, Office of Basic Energy Sciences, under Contract No. DE-AC02-06CH11357; we thank Dr Gregory J. Halder. We thank the International Synchrotron Access Program (ISAP) for funding. Use of the Australian Synchrotron was undertaken at MX-1.

Notes and references

1 O. Kahn and C. J. Martinez, *Science*, 1998, **279**, 44–48.
2 P. Gütlich and H. A. Goodwin, *Top. Curr. Chem.*, 2004, **233**, 1–47.
3 J.-F. Létard, P. Guionneau and L. Goux-Capes, *Top. Curr. Chem.*, 2004, **234**, 221–250.
4 M. A. Halcrow, *Spin-crossover materials: properties and applications*, John Wiley & Sons, Ltd., 2013.
5 P. Gütlich, A. B. Gaspar and Y. Garcia, *Beilstein J. Org. Chem.*, 2013, **9**, 342–391.
6 P. Guionneau, M. Marchivie, G. Bravic, J.-F. Létard and D. C. Chasseau, *Top. Curr. Chem.*, 2004, **234**, 97–128.
7 G. Molnár, S. Cobo, J. A. Real, F. Carcenac, E. Daran, C. Vieu and A. Bousseksou, *Adv. Mater.*, 2007, **19**, 2163–2167.
8 I. Boldog, A. B. Gaspar, V. Martínez, P. Pardo-Ibañez, V. Ksenofontov, A. Bhattacharjee, P. Gütlich and J. A. Real, *Angew. Chem., Int. Ed.*, 2008, **47**, 6433–6437.
9 T. Forestier, S. Mornet, N. Daro, T. Nishihara, S.-I. Mouri, K. Tanaka, O. Fouché, E. Freysz and J.-F. Létard, *Chem. Commun.*, 2008, 4327.
10 F. Volatron, L. Catala, E. Rivière, A. Gloter, O. Stéphan and T. Mallah, *Inorg. Chem.*, 2008, **47**, 6584–6586.
11 O. Kahn, *Molecular Magnetism*, VCH, New York, 1993.
12 S. Bonnet, M. A. Siegler, J. S. Costa, G. Molnar, A. Bousseksou, A. L. Spek, P. Gamez and J. Reedijk, *Chem. Commun.*, 2008, 5619–5621.
13 M. Nihei, H. Tahira, N. Takahashi, Y. Otake, Y. Yamamura, K. Sato and H. Oshio, *J. Am. Chem. Soc.*, 2010, **132**, 3553–3560.
14 We define here the IP thermal region as the difference between $T_{1/2}\downarrow$(cool) and $T_{1/2}\uparrow$(heat). W. Bauer, T. Pfaffeneder, K. Achterhold and B. Weber, *Eur. J. Inorg. Chem.*, 2011, 3183–3192.
15 M. Griffin, S. Shakespeare, H. J. Shepherd, C. J. Harding, J.-F. Létard, C. Desplanches, A. E. Goeta, J. A. K. Howard, A. K. Powell, V. Mereacre, Y. Garcia, A. D. Naik, H. Müller-Bunz and G. G. Morgan, *Angew. Chem., Int. Ed.*, 2011, **50**, 896–900.
16 N. F. Sciortino, K. R. Scherl-Gruenwald, G. Chastanet, G. J. Halder, K. W. Chapman, J.-F. Létard and C. J. Kepert, *Angew. Chem., Int. Ed.*, 2012, **51**, 10154–10158.
17 R. Ohtani, A. Masashi, A. Hori, M. Takata, S. Kitao, M. Seto, S. Kitagawa and M. Ohba, *J. Inorg. Organomet. Polym.*, 2013, **23**, 104–110.
18 B. J. Vieira, J. T. Coutinho, I. C. Santos, L. C. Pereira, J. C. Waerenborgh and V. da Gama, *Inorg. Chem.*, 2013, **52**, 3845–3850.
19 V. Martinez, Z. A. Castillo, M. C. Munoz, A. B. Gaspar, C. Etrillard, J.-F. Létard, S. A. Terekhov, G. V. Bukin, G. Levchenko and J. A. Real, *Eur. J. Inorg. Chem.*, 2013, 813–818.
20 Z.-Y. Li, J.-W. Dai, Y. Shiota, K. Yoshizawa, S. Kanegawa and O. Sato, *Chem.–Eur. J.*, 2013, **19**, 12948–12952.
21 J. Klingele, D. Kaase, M. Schmuker, Y. Lan, G. Chastanet and J.-F. Létard, *Inorg. Chem.*, 2013, **52**, 6000–6010.
22 J. J. Amoore, C. J. Kepert, J. D. Cashion, B. Moubaraki, S. M. Neville and K. S. Murray, *Chem.–Eur. J.*, 2006, **12**, 8220–8227.
23 M. Griffin, S. Shakespear, H. J. Shepherd, C. J. Harding, J.-F. Létard, C. Desplanches, A. E. Goeta, J. A. Howard, A. K. Powell, V. Mereacre, Y. Garcia, A. D. Naik, H. Bunz-Muller and G. G. Morgan, *Angew. Chem., Int. Ed.*, 2011, **50**, 896–900.
24 T. Kitazawa, Y. Gomi, M. Takahashi, M. Takeda, M. Enomoto and A. Miyazaki, *J. Mater. Chem.*, 1996, **6**, 119–121.
25 V. Niel, J. M. Martinez-Agudo, M. C. Munoz, A. B. Gaspar and J. A. Real, *Inorg. Chem.*, 2001, **40**, 3838–3839.
26 A. B. G. M. Seredyuk, V. Ksenofontov, M. Verdaguer, F. Villain and P. Gutlich, *Inorg. Chem.*, 2009, **48**, 6130–6141.
27 V. Martínez, A. B. Gaspar, M. C. Muñoz, G. V. Bukin, G. Levchenko and J. A. Real, *Chem.–Eur. J.*, 2009, **15**, 10960–10971.
28 P. D. Southon, L. Liu, E. A. Fellows, D. J. Price, G. J. Halder, K. W. Chapman, B. Moubaraki, K. S. Murray, J.-F. Létard and C. J. Kepert, *J. Am. Chem. Soc.*, 2009, **131**, 10998–11009.
29 G. Agusti, A. B. Gaspar, M. C. Mñnoz, P. G. Lacroix and J. A. Real, *Aust. J. Chem.*, 2009, **62**, 1155–1165.
30 R. Ohtani, K. Yoneda, S. Furukawa, N. Horike, S. Kitagawa, A. B. Gaspar, M. C. Muñoz, J. A. Real and M. Ohba, *J. Am. Chem. Soc.*, 2011, **133**, 8600–8605.
31 X. Bao, H. J. Shepherd, L. Salmon, G. Molnar, M.-L. Tong and A. Bousseksou, *Angew. Chem., Int. Ed.*, 2013, **52**, 1198–1202.
32 R. Otahani, M. Arai, H. Ohba, A. Hori, M. Takata, S. Kitagawa and M. Ohba, *Eur. J. Inorg. Chem.*, 2013, 738–744.
33 F. J. Muñoz-Lara, A. B. Gaspar, M. C. Muñoz, A. B. Lysenko, K. V. Domasevitch and J. A. Real, *Inorg. Chem.*, 2012, **51**, 13078–13080.
34 S. G. Telfer, B. Bocquet and A. F. Williams, *Inorg. Chem.*, 2001, **40**, 4818–4820.
35 C. M. Grunert, S. Reiman, H. Spiering, J. A. Kitchen, S. Brooker and P. Gütlich, *Angew. Chem., Int. Ed.*, 2008, **47**, 2997–2999.

